

## **Contrasts in calcium carbonate dissolution above the lysocline in the equatorial Indian Ocean over the last ~ 40 ka**

**Ramanand Yadav<sup>1,2</sup>, Sushant S. Naik<sup>1,2,\*</sup>, Pothuri Divakar Naidu<sup>1</sup>**

1. CSIR-National Institute of Oceanography, Dona Paula, Goa-403004, India

2. Academy of Scientific and Innovative Research (AcSIR), Ghaziabad-201002, India

\*email: sushant@nio.org ,Tel: +91 9423312268,+91 832 2450657,Fax: +91 832 2450602

### **Abstract**

Understanding calcite dissolution above the lysocline is crucial to comprehend the oceanic calcium carbonate cycle. To understand past calcite dissolution in sediments from above the lysocline, we use multiple dissolution proxies in a gravity core SSD-44/GC-01 from the central equatorial Indian Ocean, which spans a period of 43 ka. Our results suggest that calcite dissolution occurred during marine isotope stage -3 (MIS-3) and the last glacial maximum (LGM). Furthermore, dissolution of carbonate with increasing intensity occurred during the Holocene. Calcite dissolution above the lysocline is probably a result of pore water undersaturation in carbonate ion, which is in line with increased productivity during MIS-3 and the LGM. Furthermore, decreased sedimentation rate and increased exposure time of foraminifera during the Holocene may have led to efficient organic matter degradation and pore water undersaturation in carbonate ion. However, better preservation of calcite observed during the last deglacial period is probably due to increased deep-sea carbonate ion concentration, related to outgassing of CO<sub>2</sub> to the atmosphere, stored during the LGM in the deep sea.

**Keywords:** *Calcite dissolution, foraminiferal dissolution indices, lysocline, carbonate ion, central equatorial Indian Ocean.*

## 1. Introduction

It is essential to understand the oceanic calcium carbonate cycle to understand better how the oceanic environment will respond to currently increasing carbon dioxide levels. In the ocean,  $p\text{CO}_2$  and carbonate ion concentration ( $\text{CO}_3^{2-}$ ) are inversely related, which suggests that the calcite saturation state of the deep ocean, and therefore calcite preservation and dissolution, have the potential to exert significant control on atmospheric  $\text{CO}_2$  levels and global climate (Archer and Maier-Reimer, 1994). However,  $\text{CaCO}_3$  dissolution not only occurs at or below the lysocline but also in sediments above it, which is very significant from a mass balance perspective (de Villier, 2005). The consequence of supralysocline calcite dissolution is that the ocean's alkalinity response to changes in atmospheric  $\text{CO}_2$  will be faster (de Villier, 2005).

Although the sediment  $\text{CaCO}_3$  content as a function of water depth is a potential dissolution index, the relationship between the two is non-linear (Broecker, 2003). Therefore, instead of relying on a single proxy, various proxies have been used to reconstruct calcite dissolution. Dissolution indices such as coarse fraction percentage ( $>63 \mu\text{m}$ ), percentage of whole planktic foraminifera test ( $>150 \mu\text{m}$ ), benthic/planktic ratio, *Globorotalia* spp. percentage ( $>150 \mu\text{m}$ ), and percentage of radiolaria ( $>150 \mu\text{m}$ ) were used as potential proxies to study calcite dissolution on the seafloor (Oba, 1969; Peterson and Prell, 1985; Naidu, 1991). Furthermore, the foraminiferal fragmentation ratio (Le and Shackleton, 1992) was also utilized to document calcite dissolution in a deep-sea core from the equatorial Indian Ocean (Naidu and Malmgren, 1999) and the northern- South China Sea (Wang et al., 2016). Other important types of dissolution indices are based on the selective solution of the planktic foraminifera species. Selective species susceptible to dissolution get affected and modified below the foraminiferal lysocline, thus showing the dissolution intensity and preservation state (Parker, 1967; Berger, 1968, 1979; Parker and Berger, 1971; Boltovskoy and Totah, 1992). The ranking of foraminifera species based on dissolution susceptibility and their resistance to solution indicates the dissolution intensity in the deep-sea (Berger, 1968, 1970, 1979). Dissolution affects the foraminiferal ultra-structure, and its intensity leads to a breakdown of skeletal material (Be et al., 1975; Brummer, 1988; Van Kreveld, 1996; Dittert et al., 1999). The ratio of 'dissolution susceptible' to 'resistant' planktic foraminifera species was used in deep-sea cores from the tropical Indian Ocean at glacial-interglacial and orbital time scale (Naidu et al., 1993; Satpathy et al., 2020).

More recently, the shell weight of planktic foraminifera (Lohmann, 1995) and size index (Broecker and Clark, 1999) were used to estimate the deep-sea carbonate ion saturation state. Comparing these proxies showed that the shell weight proxy was more reliable of the two (Broecker

and Clark, 2001a). The size index and shell weight proxies were primarily used in the Atlantic, Pacific, and the Caribbean Sea (Broecker and Clark, 1999, 2001a, 2001b, 2001c, 2003a, 2003b, 2003c, 2003d; Broecker et al., 2001; Broecker and Clark, 2002; Barker and Elderfield, 2002; Broecker et al., 2003). Later on in the tropical Indian Ocean, various attempts were made using  $\text{CaCO}_3\%$ , size index, and shell weight to observe the dissolution intensity and estimate carbonate ion concentration during the last glacial-interglacial interval (Naidu, 1991; Naik and Naidu, 2007, 2010, 2014, Naik et al., 2014; Naik and Naidu, 2016).

Calcite dissolution in sediments above the lysocline in the equatorial Indian Ocean is not well documented. The equatorial Indian Ocean has moderate surface ocean productivity, minimal terrigenous input, and a low sedimentation rate. Hence dissolution may be the primary control on carbonate content in sediments in the past. Therefore, the equatorial Indian Ocean is unique in terms of deep-sea calcite dissolution. The foraminiferal lysocline in the equatorial Indian Ocean (~3800 m) has been established based on selected dissolution indices of planktic foraminifera (Cullen and Prell, 1984). Our study aims to understand the dissolution of carbonate in sediments from above but near to the lysocline. We utilize multiple dissolution indices from a sediment core (SSD-44/GC-01, 5°N and 77°E; water depth = 3160 m) from the central equatorial Indian Ocean (CEIO) covering the last ~ 43 ka situated above the present-day lysocline.

## **2. Regional Setting**

Core SSD-044/GC-01 recovered from the eastern flank of Cape Comorian ridge in the CEIO, from a deep abyssal region from a water depth of 3160 m. The source of sedimentation at the site is primarily biogenic particles from the overlying water column as well as pelagic clays. Due to its distant location from the Indian continental landmass, the terrestrial input in the deep-sea region of the CEIO is negligible. The core site is situated just above the present-day lysocline depth of ~ 3800 m (Cullen and Prell, 1984). The CEIO is also influenced by deep-water circulation in the form of Antarctic Circumpolar Current (ACC), which is a mixture of North Atlantic Deep Water (NADW) and Antarctic Bottom Water (AABW) (Piotrowski et al., 2009).

The surface ocean circulation of the CEIO is influenced by both summer as well as winter monsoon (Shankar et al., 2002). During the summer monsoon season, Site SSD-044/GC-01 is influenced by the Arabian Sea high-salinity water (ASHSW) carried by the West India Coastal Current (WICC) (Prasanna Kumar et al., 2004). This region is moderately productive compared to other high productive regions like the southwest Arabian Sea and the northeast Arabian Sea (Schulte et al., 1999), and current productivity conditions in this region are most elevated during the

southwest (SW) monsoon. Upwelling conditions are not so well expressed at the site due to local precipitation during the summer monsoon, and moderately upwelled water is generally overlain by low saline water (Schulte et al., 1999). During the winter monsoon, as the wind system reverses, the East India Coastal Current (EICC) forms in the north-western Bay of Bengal (BoB) and flows equatorward to join the Winter Monsoon Current (WMC), south of Srilanka. During the winter monsoon, this region is influenced by low saline water from the BoB carried by the EICC (Schott and McCreary, 2001). Productivity conditions during the wintertime are influenced by the EICC that brings in nutrient-enriched waters from the BoB (Prasanna Kumar et al., 2004).

### **3. Material and Methods**

#### **3. a. Core and Chronology**

Core SSD-044/GC-01 (5°N & 77°E) is situated ~400 km off Kanyakumari and comes under open (pelagic) ocean conditions. This 1.5 m core was sub-sampled at 1 cm interval, and the age model was established based on linear interpolation between 4 AMS radiocarbon dates (Table 1; recalculated from Yadav et al., 2021) which covers a period of ~43 ka. Dating was performed on selected planktic foraminifera species, viz, *Globigerinoides sacculifer*, *Globigerinoides ruber*, *Globorotalia menardii*, and *Neogloboquadrina dutertrei*. The calibration from radiocarbon dates to calendar age was done using the calib 8.2 program (Heaton et al., 2020). The average reservoir age of the 7 nearest locations to the study region (St. Nos. 601, 602, 603, 604- Southon et al., 2002; St. Nos. 610, 608, 609- Dutta et al., 2001) is 405.57 yr and Weighted Mean  $\Delta R = -77 \pm 58$  and age model is provided in Table 1. The sedimentation rate between 150 and 100 cm is estimated to be 4.30 cm/ka which covers a part of MIS-3. Similarly, between the 100 and 50 cm the sedimentation rate decreases slightly to 4.12 cm/ka, which is a part of MIS-3 and MIS-2 (LGM). Again between the 50 cm to top of the core, the sedimentation rate is 2.77 cm/ka which is a part of MIS-2 and the entire MIS-1. This portion displays the lowest sedimentation rate. Lithology of the core consists of a sequence of dark yellowish brown -light olive grey to olive grey colour of calcareous ooze, rich with clay, and interbedded with mixed silty-clay.

#### **3. b. processing of sediment sample for foraminiferal abundance and ranking of species based on solution susceptible and resistant species.**

For census counts of foraminifera, ~10-12 gm bulk sediment were taken on petri-dishes and oven-dried at 50 °C, overnight. The dried sediment was weighed and soaked in distilled water for 24 hrs. The soaked sediment was sieved through a 63 µm wet sieve. The coarse residue fraction (CF; >63 µm) was retained on the sieve and transferred to small beakers and oven-dried overnight. The

oven-dried residue (CF) was weighed and carefully transferred to plastic vials. The percentage of CF was estimated using the weight of dried coarse fraction divided by the weight of total dry sediment and multiplied by hundred. For planktic foraminiferal studies, a portion of CF (>125  $\mu\text{m}$ ) was dry-sieved and split many times to obtain a minimum of ~300 intact tests using a stereo zoom microscope (MEIJI-EMZ 5TR). Based on census counts, the numerical abundance (absolute abundance) of planktic foraminifera was calculated. For the species identification of planktic foraminifera, the taxonomic concept of Kennett and Srinivasan (1983) and Hemleben et al. (1989) were followed.

To check the degree of calcite dissolution, we examined the absolute abundance of common solution-susceptible species (*Globigerinoides ruber*, *Globigerinoides sacculifer*, *Globigerina bulloides*, *Globigerinita glutinata*, and *Globigerina rubescence*), solution-resistant species (*Neogloboquadrina dutertrei*, *Pulleniatina obliquiloculata*, *Globorotalia menardii*, and *Globorotalia tumida*) and the ratio of solution-susceptible species to solution-resistant species (Berger, 1968, 1970, 1979; Naidu et al., 1993; Satpathy et al., 2020). We also calculated the dissolution index (DI/ Berger Index), which is the number of tests of resistant species / total number of common species  $\times 10$ , following Berger (1973).

### ***3. c. Estimation of total carbon, total nitrogen, CaCO<sub>3</sub>% along with foraminiferal based dissolution indices, radiolarian %, shell weight analysis of selected planktic foraminifera and calculation of in-situ carbonate ion***

Finely ground sediment samples were used to analyze total carbon (TC) and total inorganic carbon (IC). The total inorganic carbon content was determined with a coulometer (UIC, Inc-CM140 acidification module) at the CSIR-National Institute of Oceanography, Goa. Analytical grade calcium carbonate was used as standard reference material. The precision of measurements was better than  $\pm 2\%$  ( $1\sigma$ ). The total inorganic carbon was converted into CaCO<sub>3</sub>% by multiplying with 8.333 (Bernard et al., 1995). Total carbon and total nitrogen (TN) were measured on a Shimadzu-Total Organic Carbon Analyser; Model: TOC LCPH at the CSIR-NIO. The results have a precision within  $\pm 3\%$  ( $1\sigma$ ) as obtained for the NC soil standard. Organic Carbon (C-org) was calculated as the difference between TC and IC.

The *Globorotalia* spp. percentage is composed of *G. menardii*, *G. tumida*, and *G. menardii neoflexuosa*. Reason behind taking *Globorotalia* spp. as common representative of above three species is, they all having keel structure on their test and after dissolution the keel becomes a part of the fragments. It is then hard to identify which species the keel belongs to. Foraminifera

fragmentation % (>125  $\mu\text{m}$ ) was calculated using the method of Le and Shackleton (1992). Radiolarian percentage was estimated as number of whole radiolarian tests in total radiolarian tests plus number of whole planktic foraminifera tests. Considered as a residual fraction, the abundance of radiolarians contains information on the amount of carbonate dissolved from this size class (Peterson and Prell, 1985). The index increases primarily through the preferential loss of planktic foraminifera (Peterson and Prell, 1985). The size index percentage was calculated as the ratio of  $\text{CaCO}_3$  in >63  $\mu\text{m}$  to that in total  $\text{CaCO}_3\%$  in bulk sediments multiplied by 100 (Broecker and Clark, 1999). Carbonate ion concentrations were normalized to a depth of 4 km following the method of Broecker and Clark (1999), as follows:

$$\text{CO}_3^{=*} = \text{CO}_3^{\ominus} + 20(4 - h)$$

Where 'h' is the water depth in km at the core site and 20  $\mu\text{mol/kg/km}$  is the increase with water depth in the solubility of calcite.  $\text{CO}_3^{=*}$  is used to avoid the necessity of selecting a value for the increasing solubility of calcite with pressure and hence water depth.

For the analysis of shell weights of selected planktic foraminifera, a portion of the CF was adequately cleaned and sonicated. The >63  $\mu\text{m}$  residue was dry sieved between 300-355 $\mu\text{m}$  size fractions. Approximately fifty shells of *G. ruber*, *P. obliquiloculata*, and *N. dutertrei* were picked and weighed on a microbalance (1 $\sigma$  precision:  $\pm 2 \mu\text{g}$ ,  $n = 10$ ). The scanning electron micrographs were obtained on a JEOL SEM 5800LV (Model: EOL/JMS) instrument at the CSIR-NIO.

The in-situ  $[\text{CO}_3^{2-}]$  (Fig. 1b) was calculated using parameters such as total alkalinity, total carbon dioxide, nutrients, including phosphate ( $\text{PO}_4$ ), silicate ( $\text{SiO}_3$ ), bottom water temperature (BWT), and salinity (S) of stations closest to the core site from the Global Ocean Data Analysis Project (GLODAP) (Key et al., 2004) and the calculations were done using the CO2sys.xls (Ver. 12) program (Pierrot et al., 2006). The constants used in the program are K1 and K2–Millero (2010),  $\text{KSO}_4$  – Dickson (1990), B and Chlorinity - Lee et al. (2010), and pH in Total Scale. The  $[\text{CO}_3^{\ominus}]$  of seawater at the core depth is  $\sim 83 \mu\text{mol/kg}$  (Fig. 1b). Further, the in-situ  $\text{CO}_3^{\ominus}$  concentration was used to calculate pressure normalized  $\text{CO}_3^{=*}$  (Broecker and Clark, 1999; Naik and Naidu, 2007; Naik and Naidu, 2010).

#### 4. Results

The percentage of  $\text{CaCO}_3$  varies from 48 % to 62 % through the 43 ka timespan. It was higher in the early MIS-3, lower during late MIS-3, increased during the LGM, and further decreased till about  $\sim 15$  ka, after which  $\text{CaCO}_3$  % showed a substantial increase, which continued into the

Holocene (Fig 2A). The C-org/Total Nitrogen ratio varied from 0 to 15% and was highest during MIS-3 followed by a slight decrease during MIS-2 and MIS-1 (Fig. 2B). The C/N values are within those reported for marine sedimentary organic matter (Reichart et al., 1997). Similarly, we estimated the CF %, composed of biogenous remains, with no lithogenous fraction (sand grains) in the last 43 ka timespan. The coarse fraction shows values of < 18 % from 43 to ~15 ka (entire MIS-3 and major part of the MIS-2) (Fig. 2C). From ~15 ka onwards, during the latter part of MIS-2 and the entire MIS-1, the CF increases. The size index % varies from ~ 20 to ~ 40 with values of <31 between 43 to ~15 ka (Fig.2C). The size index increases sharply after ~15 ka and shows a sharp decrease through the Holocene. Both the CF and size index % show a similar profile for the entire 43 ka period. When dissolution proceeds, the pressure-normalized  $\text{CO}_3^{2-}$  concentration, calculated based on the size index, falls to values below 105  $\mu\text{mol/kg}$  (Broecker and Clark, 1999). The value of  $\text{CO}_3^{2-}$  derived at our core site is 100  $\mu\text{mol/kg}$  (<105  $\mu\text{mol/kg}$ ), which suggests that our core site experiences calcite dissolution. The absolute abundance of total planktic foraminiferal number (TPN) varies from ~52,000/g to 25,000/g (Fig.2D). The total planktic foraminiferal number shows a decreasing pattern during the LGM, increasing during the deglaciation, and a further decrease through the Holocene.

The planktic foraminifera fragment % shows varying values during the MIS-3 and the LGM a further decrease during the deglaciation except for a single point, and an increase through the Holocene (Fig.2E). The benthic/planktic foraminifera ratio varies within a minimum of 0.3 and maximum of 4.8 and shows an overall rise during MIS-3, LGM and Holocene and decreases during the deglaciation (Fig. 2F). The *Globorotalia* spp. % varies between 15 % to 60 %, remains low in MIS-3 and LGM, and increases during the deglaciation, with a further decrease into the Holocene (Fig. 2G). The radiolarian percentage averaged 5 % for the entire 43 ka and showed a gentle decline from MIS-3 into the last deglaciation and a sharp increase through the Holocene (Fig. 2H).

The ratio of dissolution susceptible to dissolution resistant species shows an opposite trend to the dissolution index. It varies from ~1 to 5 and shows an increase through MIS-3 (Fig.3A). Further, this ratio shows lower values during the LGM, increases sharply during the deglacial, and decreases in the Holocene. The dissolution index varies from 1.2 to 4.4 with a reduction from MIS-3 to MIS-2 (Fig.3B). There is a sharp decrease just after the LGM and an increase through the Holocene. Shell weights of *G. ruber* range between ~ 13  $\mu\text{g}$  and ~ 16  $\mu\text{g}$ , while that of *P. obliquiloculata* vary from ~13  $\mu\text{g}$  to ~20  $\mu\text{g}$  and shell weight of *N. dutertrei* vary from 16  $\mu\text{g}$  to ~ 25  $\mu\text{g}$ . All three species' shell weights show a similar overall trend for the last 43 ka, showing a significant decrease later to ~ 15 ka, through the Holocene (Fig.4A, B, C). The Holocene decrease in shell weights is ~ 4  $\mu\text{g}$  for *G. ruber*, ~ 8  $\mu\text{g}$  for *P. obliquiloculata*, and ~ 9  $\mu\text{g}$  for *N. dutertrei*.

## 5. Discussion

It is well known that the  $\text{CaCO}_3$  content in deep-sea sediment depends on surface ocean productivity, dissolution in the water column, and the seafloor and dilution through terrigenous input. The  $\text{CaCO}_3$  of the deep sea (deeper than 1000-1200 m) is mainly contributed by calcite made up of foraminifera and coccolithophores (Kolla et al., 1976). At our study location, the surface ocean productivity conditions are moderate (Yadav et al. 2021), C-org/ TN ratio shows values  $<15$  during the last 43 ka that represents the marine source of organic matter (Meyers, 1997) (Fig. 3B). The CF is devoid of any sand-sized particles, which support the insignificant lithogenic input at the core site (Naidu and Malmgren, 1999).

The carbonate compensation depth in the Indian Ocean is  $\sim 4600$  m (Banakar et al., 1998). In a site from the Maldives Sea, which is close to our core site, the equilibrium saturation horizon ( $\Omega$  value of 1) was found at a water depth of 3684 m (Schulte and Bard, 2003). Hence the foraminiferal (calcite) lysocline depth in this region ( $\Omega = 0.8$ ) is around 4000 m (Schulte and Bard, 2003). The lysocline depth is in close agreement with Cullen and Prell (1984), which is  $\sim 3800$  m for the equatorial Indian Ocean. Hence our core site is situated above the lysocline depth. However, an earlier study from the Indian Ocean had shown dissolution to proceed from depths below  $\sim 2300$  m (Naik and Naidu, 2007; 2008), which can be on the seafloor itself, before burial called as interface dissolution or after burial, also known as pore water dissolution. The pore water dissolution is driven by releasing  $\text{CO}_2$  due to respiration (Emerson and Bender, 1981).

To understand calcite dissolution at specific periods, we mainly rely on the foraminifera-based dissolution proxies. The ranking of planktic foraminiferal species based on their selective solution has been classified with respect to depth, susceptibility of dissolution, and distance from the equator (Berger, 1968) (Fig. 3). The less resistant species having macropores, spines, and thinner tests usually flourished near the sea surface. The dissolution-resistant species having thick walls and smooth tests flourished in upper to deep thermocline (Arrhenius, 1952; Phleger et al., 1953; Berger, 1967). Here the species are classified into two major groups, common dissolution susceptible species and common solution resistant species based on their relative susceptibility to dissolution (Sd). The Sd of some species are: *G. ruber* = 0.22, *G. bulloides* = 0.34, *G. glutinata* = 1.2, *P. obliquiloculata* = 5 and *G. tumida* = 15 (Conan et al., 2002).

The shell weights of planktic foraminifera may initially depend on several factors such as surface water carbonate ion and optimal growth conditions (de Villier, 2005; Beer et al., 2010; Naik and Naidu, 2010; Naik et al., 2013). After settling to the ocean floor, the planktic foraminifera are



affected by the bottom-water carbonate ion saturation (Broecker and Clark, 1999). The bottom water saturation state in turn reflects pore water undersaturation. We have employed three planktic foraminifera; first, *G. ruber*, which generally flourishes in surface water or the mixed layer depth and is known to be solution susceptible, as the test of this particular species is quite delicate (Parker, 1967; Berger, 1968). It has macropores and has spines at its surface (Conan et al., 2002). Second, *P. obliquiloculata*, which flourishes within the thermocline and shows secondary calcification. The test of this particular species is thick, smooth, and known to be solution resistant (Parker, 1967; Berger, 1968). Third, *N. dutertrei*, which also flourishes in the upper thermocline, has a thick wall, shows secondary calcification, and belongs to the dissolution resistant group of faunal classification. In general, though the three foraminifera species used here are from different depth habitats, the shell weight trend shows a similar pattern, which suggests the bottom-water carbonate ion undersaturation is the prime reason for their broad trend.

### 5.2.1 Carbonate dissolution during MIS-3 and the LGM

During the MIS-3 and the LGM, dissolution indices support calcite dissolution. The TPN shows low values during the MIS-3 (except later portion of MIS-3) and the LGM. The *Globorotalia* spp. percentage and the size index also show lower values for this period except during the last portion of MIS-3. When dissolution proceeds, the thin chamber of the species of the *Globorotalia* spp. dissolves first, and the thick keel is left, which becomes part of the fragments. Hence lower percentage of *Globorotalia* spp. signifies dissolution. The size index range from ~ 20 to 40 between 43 to 19 ka, which corresponds to a  $\text{CO}_3^{*}$  of 80 to 90  $\mu\text{mol/kg}$ , is in the range wherein calcite dissolution occurs (Broecker and Clark, 1999). The fragment percentage and the benthic/planktic ratio shows higher than average values during MIS-3 and the LGM. As benthic foraminifera are more resistant than planktic, lower ratios signify dissolution. The benthic/planktic ratio displays an opposite trend to the *Globorotalia* spp. percentage. Radiolarian percentage shows slightly higher values during MIS-3 than the LGM, although they are not much significant. Radiolarian percentage from  $>125 \mu\text{m}$  is considered as a residual fraction that is the noncarbonated component that contains the information about dissolved calcite (Peterson and Prell, 1985). The ratio of the dissolution susceptible to resistant species shows an increasing trend through MIS-3 with a decrease at ~ 30 ka and during the LGM (Fig. 3A). The dissolution index shows a decreasing trend through MIS-3 with an increase at ~ 30 ka and a slight increase during the LGM (Fig. 3B). The shell weights of *G. ruber* show overall higher shell weights with large fluctuations during MIS-3 and lowered shell weights during the LGM, while *P. obliquiloculata* and *N. dutertrei* show overall higher shell weights with

large fluctuations and an increasing trend through the MIS-3 and LGM with lowered shell weights in the later part of the LGM (Fig.4A, B, C).

All our proxies suggest deep-sea calcite dissolution in the study region during the MIS-3 and the LGM, albeit with a comparatively increased intensity during the LGM. Calcite dissolution is evident in the SEM micrographs of *G. ruber* at ~ 22 ka, which shows peeling of surface and dissolution of spines (Fig. 5C). Dissolution of carbonate during the LGM may be related to inadequate deep-water ventilation at the core site due to reduced proportion of O<sub>2</sub> rich NADW and increased proportion of AABW that was CO<sub>2</sub> rich and O<sub>2</sub> poor (Ahmad et al., 2008; Piotrowski et al., 2009; Chandana et al., 2017). Our faunal proxy and C-org content reveal that productivity was high during MIS 3 and 2, especially during the LGM (Yadav et al., 2021). The calcite dissolution during MIS 3 and the LGM is probably related to increased productivity, leading to increased organic matter export to the sediments. Degradation of this organic matter in sediments can lead to increased CO<sub>2</sub> and undersaturation with respect to carbonate ion that finally reduced the preservation of CaCO<sub>3</sub> in the study region (Emerson and Bender, 1981; Archer et al., 1989; Hales et al., 1994; Hales and Emerson, 1997).

### **5.2.2 Increased calcite preservation observed during the last deglacial period**

Between the 19-12 ka period, the CF and the TPN showed a significant increase (Fig.2C, D). The *Globorotalia* spp. and the size index percentage both show a sharp increase. The fragment percentage and the benthic/planktic ratio show lower values, except for a single point showing a high fragment percentage. The radiolarian percentage shows the lowest values during the deglaciation. The ratio of the dissolution susceptible to resistant species and the dissolution index shows the lowest and highest values, respectively (Fig. 3A and B). Interestingly, the shell weights of *G. ruber* and *N. dutertrei* display the highest and lowest shell weights during this period (Fig. 4). The decreased shell weights observed at ~ 15 ka may be related to the CO<sub>2</sub> degassing and decreased surface water carbonate ion content in the northern Indian Ocean (Naik and Naik, 2018).

All these proxies point towards increased preservation (decreased dissolution) of calcite during the last deglacial period. Scanning electron micrographs of *G. ruber* at ~ 16 ka show well-preserved spines supporting increased calcite preservation during the last deglacial period (Fig. 5A). The carbonate preservation suggests increased deep-water carbonate ion concentrations during the deglaciation. Such preservation has been documented across the world's oceans, including the northern Indian Ocean, at various water depths (Naik and Naidu, 2016). Atmospheric CO<sub>2</sub> levels increased during the deglaciation due to the breakdown of stratification, releasing CO<sub>2</sub> stored in the

deep ocean to the atmosphere (Anderson et al., 2009). The release of deeply stored CO<sub>2</sub> leads to an increase in deep-sea carbonate ion concentration (Yu et al., 2014).

### 5.2.3 Intense calcite dissolution during the Holocene

Our multi-proxy approach suggests calcite dissolution with increasing intensity through the Holocene epoch. The CF and the TPN show a decreasing trend. The *Globorotalia* spp. percentage shows varying values, and the size index shows a decreasing trend. The size index values are higher during the Holocene in comparison to the MIS-3 and LGM. The size index has limitations when applied to sediments from above the lysocline, recovered from regions or periods dominated by coccolithophores (Naik and Naidu, 2010), which we have not estimated for the present study. Similarly, if the MIS-3 and LGM were dominated by coccolithophores and the Holocene dominated by foraminifera, the CF would not give a correct indication of calcite dissolution. The fragment percentage, the benthic/planktic ratio, and radiolarian percentage show an increasing trend. The dissolution index shows an increasing trend, whereas the ratio of the dissolution susceptible to resistant species shows a decreasing trend (Fig. 3B and A). Interestingly, the shell weights of *G. ruber*, *P. obliquiloculata*, and *N. dutertrei* show a sharp decline through the Holocene (Fig. 4).

All these proxies support calcite dissolution during the Holocene, with increasing intensity from early to late Holocene although the CaCO<sub>3</sub> content is high. The variability in calcium carbonate for the last 43 ka is only within 10%. Data from the same core shows that carbonate production decreased during the Holocene (Yadav et al., 2021). The increased carbonate content seen during the Holocene is most likely due to advection of eroded carbonate material from the Maldives coral reefs (Tang et al., 2020). Calcite dissolution is evident in the SEM micrographs of *G. ruber*, which show peeling of surface and dissolution of spines (Fig. 5a). It has been shown that calcite dissolution starts to affect planktic foraminifera from >2250 m depth (Naik and Naidu, 2007; 2008). The data from the present study is in line with earlier studies showing the dissolution of calcite above the lysocline depth as a result of bottom water undersaturation with respect to carbonate ion. Conversely, intense dissolution at the core site could probably be a result of lowered carbonate ion concentration in pore waters due to organic matter degradation. Overall, the surface productivity was low later to the LGM at the core site (Yadav et al., 2021). The low sedimentation rates led to a higher exposure time of foraminifera to undersaturated waters. It is plausible that although productivity remained low, organic matter was efficiently degraded during the Holocene as a result of well-oxygenated bottom waters (NADW) reaching the core site, which is in contrast to the LGM conditions of an increased proportion of AABW which is O<sub>2</sub> deficient (Chandana et al., 2017). Thus degradation of organic

matter on the sea-floor and in the sediments must have led to undersaturation of pore waters and more intense calcite dissolution.

From the LGM to the Holocene, sea level rose by 120 m. A lowered sea-level reduces the available neritic area and thus reduces carbonate accumulation, inducing a higher  $\text{CO}_3^{2-}$  and a lower  $\text{CO}_2$  (Berger, 1982; Ridgwell et al., 2003). Thus a low sea-level corresponds to a deeper lysocline (MIS-3-deep and LGM-deepest) and high sea-level corresponds to a shallower lysocline (Holocene). The SSD-044/GC-01 core is situated presently at a water depth of 3160 m which is at least ~700 m above the present day lysocline in this region. Previous study by Farrell and Prell, 1989, has showed that the glacial-interglacial variation in lysocline was in the range of 400 to 800 m for the last 0.8 Ma. Applying this variability to our core depth, the lysocline was probably at ~ 4200 during the LGM. Hence we can safely assume that our core site was always above the lysocline through the study period of 43 ka. Hence calcite dissolution due to variations in the lysocline depth can be ruled out.

## **6. Conclusion**

In an attempt to understand deep-sea calcite dissolution above the lysocline, we have applied multiple dissolution proxies to a core raised from the central equatorial Indian Ocean, covering a period of the last 43 ka. Here, all the proxies- dissolution indices, the ratio of dissolution susceptible to dissolution resistant species, dissolution index, size index, and shell weights of selected planktic foraminifera show that calcite dissolution occurred with varying intensity through the marine isotope stage-3 and slightly increased intensity during the last glacial maximum. Furthermore, we could identify calcite dissolution with increasing intensity through the Holocene. The most viable explanation for this supralysoclineal calcite dissolution is pore-water undersaturation with respect to carbonate ion due to organic matter degradation. However, better preservation of calcite was observed during the last deglaciation, probably related to the release of carbon from the deep ocean during the last glacial maximum and the associated rise in deep-sea carbonate ion.

## **7. Data Availability**

Datasets related to this article can be found in the institute's data repository: <https://publication-data.nio.org/s/npAnd43P5eQPcAB>

## **Acknowledgements**

The authors are thankful to the Director, CSIR-National Institute of Oceanography, Goa, India, for infrastructural support and permission to publish this work. We thank the ship cell, NIO, captain,

and crew members of RV Sindhu Sadhana (SSD-044) for their assistance during the cruise. We are thankful to Teja Naik for her help in total nitrogen and carbon analysis under the Central Analytical Facility (CAF) of the CSIR-NIO, Goa, India. Areef Sardar (NIO) is thankfully acknowledged for the SEM images and Smita Naik for the carbonate ion calculations. This core was obtained as a part of the MoES project 'Biogeochemical Process and Paleoceanographic Studies of the Eastern Indian Ocean.' RY is thankful for providing the research fellowship (CSIR-SRF, Grant No.31/026(0291)/2016-EMR-I). We thank the Editor Dr. Adina Paytan and two anonymous reviewers for constructive comments and suggestions, which helped us to improve the manuscript. This is National Institute of Oceanography contribution No. XXXX.

## References

- Ahmad, S.M., Babu, G.A., Padmakumari, V.M., Raza, W., 2008. Surface and deep water changes in the northeast Indian Ocean during the last 60 ka inferred from carbon and oxygen isotopes of planktonic and benthic foraminifera. *Palaeogeogr. Palaeoclimatol. Palaeoecol.* 262,182-188.<https://doi.org/10.1016/j.palaeo.2008.03.007>.
- Anderson, R. F., Ali, S., Bradtmiller, L. I., Nielsen, S. H. H., Fleisher, M. Q., Anderson, B. E., & Burckle, L. H. (2009). Wind-driven upwelling in the Southern Ocean and the deglacial rise in atmospheric CO<sub>2</sub>. *Science*, 323(5920), 1443-1448. <https://doi.org/10.1126/science.1167441>.
- Archer D., Emerson S., Reimers, C., 1989. Dissolution of calcite in deep-sea sediments: pH and O<sub>2</sub> microelectrode results. *Geochim. Cosmochim. Acta* 53, 2831–2845.[https://doi.org/10.1016/0016-7037\(89\)90161-0](https://doi.org/10.1016/0016-7037(89)90161-0).
- Archer, D., Maier-Reimer, E., 1994. Effect of deep-sea sedimentary calcite preservation on atmospheric CO<sub>2</sub> concentration. *Nature*, 367, 260-263. <https://doi.org/10.1038/367260a0>.
- Arrhenius, G., 1952. Sediment cores from the east Pacific. *Reports Swedish Deep-Sea Expedition 1947-1948*, 5, 1-228.
- Banakar, V.K., Parthiban, G., Pattan, J.N., Jauhari, P., 1998. Chemistry of surface sediment along a north–south transect across the equator in the Central Indian Basin: an assessment of biogenic and detrital influences on elemental burial on the seafloor. *Chemical Geology*, 147, 217-232. [https://doi.org/10.1016/S0009-2541\(98\)00015-1](https://doi.org/10.1016/S0009-2541(98)00015-1).
- Barker, S., Elderfield, H., 2002. Foraminiferal calcification response to glacial-interglacial changes in atmospheric CO<sub>2</sub>. *Science*, 297(5582), 833-836.<https://doi.org/10.1126/science.https://doi.org/10.1126/science.1072815>.
- Be., A.W.H., Morse, J.W., Harrison, S.M., 1975. Progressive dissolution and ultrastructural breakdown of planktic foraminifera. In: Sliter, W.V., Be., A.W.H., Berger, W.H. (Eds.), *Dissolution of Deep-Sea Carbonates*. Cushman Foundation, Spec. Publ. No. 13. Allen Press, Kansas, 27-55.

- Beer, C.J., Schiebel, R., Wilson, P.A., 2010. Testing planktic foraminiferal shell weight as a surface water [CO<sub>2</sub>] proxy using plankton net samples. *Geology*, 38, 103-106. <http://dx.doi.org/10.1130/G30150.1>.
- Berger, W.H., 1967. Foraminiferal ooze: solution at depths. *Science*, 156, 383-385. <https://doi.org/10.1126/science.156.3773.383>.
- Berger, W.H., 1968. Planktonic foraminifera: selective solution and paleoclimatic interpretation. *Deep-Sea Res.* 15, 31-43. [https://doi.org/10.1016/0011-7471\(68\)90027-2](https://doi.org/10.1016/0011-7471(68)90027-2).
- Berger, W.H., 1970. Planktonic foraminifera: selective solution and the Lysocline. *Mar. Geol.* 8(2), 111-138. [https://doi.org/10.1016/0025-3227\(70\)90001-0](https://doi.org/10.1016/0025-3227(70)90001-0).
- Berger, W.H., 1973. Deep-sea carbonates: Pleistocene dissolution cycles. *J. Foraminifer. Res.* 3, 187-195. <https://doi.org/10.2113/gsjfr.3.4.187>.
- Berger, W.H., 1979. Preservation of foraminifera. In: *Foraminiferal Ecology and Paleoecology*, SEPM Short Course No. 6. Houston, TX, 105-155.
- Berger, W.H., 1982. Increase of carbon dioxide in the atmosphere during deglaciation: the coral reef hypothesis. *Naturwissenschaften* 69 (2), 87e88.
- Bernard, B.B., Bernard, H., Brooks, J.M., 1995. Determination of total carbon, total organic carbon and inorganic carbon in sediments. TDI-Brooks International/B&B Laboratories Inc. College Station, Texas, pp.1-5.
- Boltovskoy, E., Totah, V., 1992. Preservation index and preservation potential of some foraminiferal species. *J. Foraminifer. Res.* 22, 267-273. <https://doi.org/10.2113/gsjfr.22.3.267>.
- Broecker, W.S., Clark, E., 1999. CaCO<sub>3</sub> size distribution: A paleocarbonate ion proxy?. *Paleoceanography*, 14, 596-604. <https://doi.org/10.1029/1999PA900016>.
- Broecker, W., Clark, E., 2001a. An evaluation of Lohmann's foraminifera weight dissolution index. *Paleoceanography*, 16, 531-534. <https://doi.org/10.1029/2000PA000600>.
- Broecker, W.S., Clark, E., 2001b. Glacial-to-Holocene redistribution of carbonate ion in the deep sea. *Science*, 294, 2152-2155. <https://doi.org/10.1126/science.1064171>.
- Broecker, W.S., Clark, E., 2001c. Reevaluation of the CaCO<sub>3</sub> size index paleocarbonate ion proxy. *Paleoceanography*, 16, 669-671.
- Broecker, W.S. and Clark, E., 2002. Carbonate ion concentration in glacial-age deep waters of the Caribbean Sea. *Geochem. Geophys. Geosyst.* 3, 1-14. <https://doi.org/10.1029/2001GC000231>.
- Broecker, W.S., 2003. The oceanic CaCO<sub>3</sub> cycle. In: Holland, H.D., Turekian, K.K. (Eds.), *Treatise on Geochemistry*. Elsevier, Amsterdam, pp. 529–549.
- Broecker, W.S., Clark, E., 2003a. CaCO<sub>3</sub> dissolution in the deep sea: Paced by insolation cycles. *Geochem. Geophys. Geosyst.* 4(7), 1059. <https://doi.org/10.1029/2002GC000450>.
- Broecker, W.S., Clark, E., 2003b. Holocene atmospheric CO<sub>2</sub> increase as viewed from the seafloor. *Global- Biogeochem. Cycles.* 17(2), 1052. <https://doi.org/10.1029/2002GB001985>.

- Broecker, W.S., Clark, E., 2003c. Glacial-age deep sea carbonate ion concentrations. *Geochem. Geophys. Geosyst.* 4(6), 1047. <https://doi.org/10.1029/2003GC000506>.
- Broecker, W.S., Clark, E., 2003d. Pseudo dissolution of marine calcite. *Earth Planet. Sci. Lett.* 208, 291-296. [https://doi.org/10.1016/S0012-821X\(03\)00051-7](https://doi.org/10.1016/S0012-821X(03)00051-7).
- Broecker, W.S., Clark, E., Droxler, A.W., 2003. Shell weights from intermediate depths in the Caribbean Sea. *Geochem. Geophys. Geosyst.* 4(7), 1060. <https://doi.org/10.1029/2002GC000491>.
- Broecker, W.S., Lynch-Stieglitz, J., Clark, E., Hajdas, I., Bonani, G., 2001. What caused the atmosphere's CO<sub>2</sub> content to rise during the last 8000 years?. *Geochem. Geophys. Geosyst.* 2(10). <https://doi.org/10.1029/2001GC000177>.
- Brummer, G.J.A., 1988. Comparative ontogeny of modern microperforate planktic foraminifera. In: Brummer, G.J.A., Kroon, D. (Eds.), *Planktic Foraminifers as Tracers of Ocean-Climate History*. Double Ph.D. Thesis, Free University Press, Amsterdam, Free University, Amsterdam, 77-129.
- Chandana, K.R., Bhushan, R., Jull, A.J.T., 2017. Evidence of poor bottom water ventilation during LGM in the equatorial Indian Ocean. *Front. Earth Sci.* 5, 84. <https://doi.org/10.3389/feart.2017.00084>.
- Conan, S.H., Ivanova, E.M., Brummer, G.J., 2002. Quantifying carbonate dissolution and calibration of foraminiferal dissolution indices in the Somali Basin. *Mar. Geol.* 182, 325-349. [https://doi.org/10.1016/S0025-3227\(01\)00238-9](https://doi.org/10.1016/S0025-3227(01)00238-9).
- Cullen, J.L., Prell, W.L., 1984. Planktonic foraminifera of the northern Indian Ocean: distribution and preservation in surface sediments. *Mar. Micropaleontol.* 9, 1-52. [https://doi.org/10.1016/0377-8398\(84\)90022-7](https://doi.org/10.1016/0377-8398(84)90022-7).
- De Villiers, S., 2005. Foraminiferal shell-weight evidence for sedimentary calcite dissolution above the lysocline. *Deep Sea Res. Part I: Oceanogra. Res. Pap.* 52, 671-680. <http://dx.doi.org/10.1016/j.dsr.2004.11.014>.
- Dickson, A. G., 1990. Thermodynamics of the dissociation of boric acid in synthetic seawater from 273.15 to 318.15 K. *Deep Sea Res. Part A. Oceanogra. Res. Pap.* 37(5), 755-766. [https://doi.org/10.1016/0198-0149\(90\)90004-F](https://doi.org/10.1016/0198-0149(90)90004-F).
- Dittert, N., Baumann, K.-H., Bickert, T., Henrich, R., Huber, R., Kinkel, H., Meggers, H., 1999. Carbonate dissolution in the deep-sea: methods, quantification and paleoceanographic application. In: Fischer, G., Wefer, G. (Eds.), *Use of Proxies in Paleoceanography: Examples from the South Atlantic*. Springer-Verlag, Berlin, 255-284.
- Dutta, K., Bhushan, R., Somayajulu, B., 2001.  $\Delta R$  correction values for the northern Indian Ocean. *Radiocarbon*, 43(2A), 483-488. <https://doi.org/10.1017/S0033822200038376>.
- Emerson, S., Bender, M., 1981. Carbon fluxes at the sediment–water interface of the deep-sea: calcium carbonate preservation. *J. Mar. Res.* 39, 139–162.

- Farrell, J.W., Prell, W.L., 1989. Climatic change and CaCO<sub>3</sub> preservation: an 800,000 year bathymetric reconstruction from the central equatorial Pacific Ocean. *Paleoceanogr.* 4 (4), 447e466.
- Hales, B., Emerson, S., 1997. Calcite dissolution in sediments of the Ceara Rise: in situ measurements of porewater O<sub>2</sub>, pH and CO<sub>2</sub> (aq). *Geochim. Cosmochim. Acta* 61, 501-514.
- Hales B., Emerson S., Archer, D., 1994. Respiration and dissolution in the sediments of the western North Atlantic: estimates from models of in situ microelectrode measurements of porewater oxygen and pH. *Deep-Sea Res.* 41, 695–719. [https://doi.org/10.1016/0967-0637\(94\)90050-7](https://doi.org/10.1016/0967-0637(94)90050-7).
- Heaton, T.J., Köhler, P., Butzin, M., Bard, E., Reimer, R.W., Austin, W.E., Ramsey, C.B., Grootes, P.M., Hughen, K.A., Kromer, B., Reimer, P.J., 2020. Marine20—the marine radiocarbon age calibration curve (0–55,000 cal BP). *Radiocarbon*, 62(4), 779-820. <https://doi.org/10.1017/RDC.2020.68>.
- Hemleben, C., Spindler, M., Anderson, O.R., 1989. *Modern Planktonic Foraminifera*. Springer-Verlag, New York, pp. 363.
- Kennett, J.P., Srinivasan, M.S., 1983. *Neogene Planktonic Foraminifera, a Phylogenetic Atlas*. Hutchinson and Ross Publications, Pennsylvania, pp. 265.
- Key, R.M., Kozyr, A., Sabine, C.L., Lee, K., Wanninkhof, R., Bullister, J.L., Feely, R.A., Millero, F.J., Mordy, C., Peng, T.H., 2004. A global ocean carbon climatology: Results from Global Data Analysis Project (GLODAP). *Global. Biogeochem. Cycles.* 18(4). <https://doi.org/10.1029/2004GB002247>.
- Kolla, V., Bé, A.W., Biscaye, P.E., 1976. Calcium carbonate distribution in the surface sediments of the Indian Ocean. *J. Geophys. Res.* 81, 2605-2616. <https://doi.org/10.1029/JC081i015p02605>.
- Le, J., Shackleton, N.J., 1992. Carbonate dissolution fluctuations in the western equatorial Pacific during the late Quaternary. *Paleoceanography*, 7, 21-42. <https://doi.org/10.1029/91PA02854>.
- Lee, K., Kim, T. W., Byrne, R. H., Millero, F. J., Feely, R. A., Liu, Y. M., 2010. The universal ratio of boron to chlorinity for the North Pacific and North Atlantic oceans. *Geochim. Cosmochim. Acta.* 74, 1801-1811. <https://doi.org/10.1016/j.gca.2009.12.027>.
- Lohmann, G.P., 1995. A model for variation in the chemistry of planktonic foraminifera due to secondary calcification and selective dissolution. *Paleoceanography*, 10, 445-457. <https://doi.org/10.1029/95PA00059>.
- Meyers, P.A., 1997. Organic geochemical proxies of paleoceanographic, paleolimnologic, and paleoclimatic processes. *Org. geochem.* 27, 213-250. [https://doi.org/10.1016/S0146-6380\(97\)00049-1](https://doi.org/10.1016/S0146-6380(97)00049-1).
- Millero, F. J. (2010). Carbonate constants for estuarine waters. *Mar. Freshw. Res.* 61, 139-142. <https://doi.org/10.1071/MF09254>.
- Naidu, P.D., 1991. Glacial to interglacial contrasts in the calcium carbonate content and influence of Indus discharge in two eastern Arabian Sea cores. *Palaeogeogra. Palaeoclimatol. Palaeoecol.* 86, 255-263. [https://doi.org/10.1016/0031-0182\(91\)90084-5](https://doi.org/10.1016/0031-0182(91)90084-5).



- Naidu, P.D., Malmgren, B.A., Bornmalm, L., 1993. Quaternary history of calcium carbonate fluctuations in the western equatorial Indian Ocean (Somali Basin). *Palaeogeogr. Palaeoclimatol. Palaeoecol.* 103, 21-30. [https://doi.org/10.1016/0031-0182\(93\)90048-N](https://doi.org/10.1016/0031-0182(93)90048-N).
- Naidu, P.D., Malmgren, B.A., 1999. Quaternary carbonate record from the equatorial Indian Ocean and its relationship with productivity changes. *Mar. Geol.* 161(1), 49-62. [https://doi.org/10.1016/S0025-3227\(99\)00055-9](https://doi.org/10.1016/S0025-3227(99)00055-9).
- Naik, S.S., Naidu, P.D., 2007. Calcite dissolution along a transect in the western tropical Indian Ocean: A multiproxy approach. *Geochem. Geophys. Geosyst.* 8(8), Q08009. <https://doi.org/10.1029/2007GC001615>.
- Naik, S.S. and Naidu, P.D., 2008. Possible factors that control calcite dissolution in the western tropical Indian Ocean. *Curr. Sci.* 95, 22- 23.
- Naik, S.S., Naidu, P.D., 2010. Evaluation of the CaCO<sub>3</sub> dissolution proxies in sediment cores from above the lysocline. *Quatern. Int.* 213, 69-73. <https://doi.org/10.1016/j.quaint.2008.11.009>.
- Naik, S.S., Godad, S.P., Naidu, P.D., Ramaswamy, V., 2013. A comparison of *Globigerinoides ruber* calcification between upwelling and non-upwelling regions in the Arabian Sea. *J. Earth Syst. Sci.*, 122, 1153-1159. <https://doi.org/10.1007/s12040-013-0330-y>.
- Naik, S.S., Naidu, P.D., 2014. Boron/calcium ratios in *Globigerinoides ruber* from the Arabian Sea: Implications for controls on boron incorporation. *Mar. Micropaleontol.* 107, 1-7. <https://doi.org/10.1016/j.marmicro.2014.01.004>.
- Naik, S.S., Godad, S.P., Naidu, P.D., Tiwari, M., Paropkari, A.L., 2014. Early-to late-Holocene contrast in productivity, OMZ intensity and calcite dissolution in the eastern Arabian Sea. *The Holocene* 24, 749-755. <https://doi.org/10.1177/0959683614526936>.
- Naik, S.S. and Naidu, P.D., 2016. Carbonate preservation during the ‘mystery interval’ in the northern Indian Ocean. *Geochem. J.* 50, 357-362. <https://doi.org/10.2343/geochemj.2.0420>.
- Naik, S.N., Naik, S.S., 2018. Evidences of CO<sub>2</sub> Leakage During the Last Deglaciation: The Need to Understand Deep-ocean Carbonate Chemistry of the Arabian Sea. *J. Geol. Soc. India* 92, 404-406.
- Oba, T., 1969. Biostratigraphy and isotopic paleotemperature of some deep-sea cores from the Indian Ocean. The science reports of the Tohoku University. Second series, Geology, 41, 129-195.
- Parker, F.L., 1967. Late Tertiary biostratigraphy (planktonic foraminifera) of tropical Indo-Pacific deep-sea cores. *Bull. Am. Paleont.* 52, 115-208.
- Parker, F.L., Berger, W.H., 1971. Faunal and solution patterns of planktonic foraminifera in surface sediments of the South Pacific. *Deep-Sea Res.* 18, 73-107. [https://doi.org/10.1016/0011-7471\(71\)90017-9](https://doi.org/10.1016/0011-7471(71)90017-9).
- Peterson, L.C., Prell, W.L., 1985. Carbonate dissolution in recent sediments of the eastern equatorial Indian Ocean: preservation patterns and carbonate loss above the lysocline. *Mar. Geol.* 64, 259-290. [https://doi.org/10.1016/0025-3227\(85\)90108-2](https://doi.org/10.1016/0025-3227(85)90108-2).

- Phleger, F.B., 1953. North Atlantic core foraminifera. Reports on the Swedish Deep-Sea Expedition, 7, 1-122.
- Pierrot, D., Lewis, E., Wallace, D.W.R., 2006. MS Excel program developed for CO<sub>2</sub> system calculations. ORNL/CDIAC-105a. Carbon Dioxide Information Analysis Center, Oak Ridge National Laboratory, US Department of Energy, Oak Ridge, Tennessee, 10.
- Piotrowski, A.M., Banakar, V.K., Scrivner, A.E., Elderfield, H., Galy, A., Dennis, A., 2009. Indian Ocean circulation and productivity during the last glacial cycle. *Earth Planet. Sci. Lett.* 285,179-189.<https://doi.org/10.1016/j.epsl.2009.06.007>.
- Prasanna Kumar, S., Narvekar, J., Kumar, A., Shaji, C., Anand, P., Sabu, P., Rijomon, G., Josia, J., Jayaraj, K.A., Radhika, A., Nair, K.K.C., 2004. Intrusion of the Bay of Bengal water into the Arabian Sea during winter monsoon and associated chemical and biological response. *Geophys. Res. Lett.* 31, L15304. <https://doi.org/10.1029/2004GL020247>.
- Ridgwell, A.J., Kennedy, M.J., Caldeira, K., 2003. Carbonate deposition, climate stability, and Neoproterozoic ice ages. *Science*, 302 (5646), 859e862. <https://doi.org/10.1126/science.1088342>
- Satpathy, R.K., Steinke, S., Singh, A.D., 2020. Monsoon-induced changes in surface hydrography of the eastern Arabian Sea during the early Pleistocene. *Geol. Mag.* 157, 1001-1011.<https://doi.org/10.1017/S0016756819001122>.
- Shankar, D., Vinayachandran, P.N., Unnikrishnan, A.S., 2002. The monsoon currents in the north Indian Ocean. *Prog. oceanogra.* 52, 63-120.[https://doi.org/10.1016/S0079-6611\(02\)00024-1](https://doi.org/10.1016/S0079-6611(02)00024-1).
- Schott, F.A., McCreary Jr, J.P., 2001. The monsoon circulation of the Indian Ocean. *Prog. Oceanogra.* 51, 1-123. [https://doi.org/10.1016/S0079-6611\(01\)00083-0](https://doi.org/10.1016/S0079-6611(01)00083-0).
- Schulte, S., Rostek, F., Bard, E., Rullkötter, J., Marchal, O., 1999. Variations of oxygen minimum and primary productivity recorded in sediments of the Arabian Sea. *Earth Planet. Sci. Lett.* 173, 205-221. [https://doi.org/10.1016/S0012-821X\(99\)00232-0](https://doi.org/10.1016/S0012-821X(99)00232-0).
- Schulte, S., Bard, E., 2003. Past changes in biologically mediated dissolution of calcite above the chemical lysocline recorded in Indian Ocean sediments. *Quat. Sci. Rev.* 22, 1757-1770. [https://doi.org/10.1016/S0277-3791\(03\)00172-0](https://doi.org/10.1016/S0277-3791(03)00172-0).
- Southon, J., Kashgarian, M., Fontugne, M., Metivier, B., Yim, W.W., 2002. Marine reservoir corrections for the Indian Ocean and Southeast Asia. *Radiocarbon*, 44(1), 167-180. <https://doi.org/10.1017/S0033822200064778>.
- Tang, L. –G., Su, X., Yang, Y. –P., Xiang, R., 2020. Sedimentary response to sea level and climate changes in the inner sea of Maldives carbonate platform over the past 30 kyr. *Palaeoworld* 30 (1-4) 573-582. <https://doi.org/10.1016/j.palwor.2020.09.003>.
- Van Kreveland, S.A., 1996. Calcium carbonate dissolution indices on the northeast Atlantic sea floor. In: van Kreveland, S.A.(Ed.), *Late Quaternary Sediment Records of Mid-latitude Northeast Atlantic Calcium Carbonate Production and Dissolution* Ph.D. Thesis, Free University, Amsterdam, FEBO B.V., Enschede, 135-184.

- Wang, N., Huang, B.Q., Li, H., 2016. Deep-water carbonate dissolution in the northern South China Sea during Marine Isotope Stage 3. *J. Palaeogeogr.* 5, 100-107. <https://doi.org/10.1016/j.jop.2015.11.004>.
- Yadav, R., Naik, S.S., Narvekar, J., 2021. The equatorial Indian Ocean upper water-column structure influenced by cross-basinal water exchange over the last~ 40000 years. *Quat. Int.* 1-9. <https://doi.org/10.1016/j.quaint.2021.04.002>.
- Yu, J., Broecker, W.S., Elderfield, H., Jin, Z., McManus, J. and Zhang, F., 2010. Loss of carbon from the deep sea since the Last Glacial Maximum. *Science*, 330, 1084-1087. <https://doi.org/10.1126/science.1193221>.

## Legend to figures

- Figure: 1** a) Map showing Core SSD-044/GC-01 recovered from the equatorial Indian Ocean, shown with a red-filled circle. GLODAP station used for calculating the carbonate ion concentration profile are shown as star; b) Carbonate ion concentration versus depth for the GLODAP station shown in (a).
- Figure: 2** Down core variations of dissolution indices for the last 43ka; (A) CaCO<sub>3</sub> percentage, (B) C/N ratio, (C) Coarse fraction (CF) (>63µm) and size index percentage, (D) Total Planktic foraminifera Number, (E) Foraminifera fragment percentage (>125µm), (F) Benthic/Planktic foraminifera ratio, (G) *Globorotalia* spp. percentage (*G. menardii*, *G. tumida*, *G. menardii neoflexuosa*) and (H) Radiolarian percentage (The Last Glacial Maximum (LGM) marked by dotted bars and Bølling Allerød (BA) is shaded in gray. The MIS-1 & MIS-3 are marked by light blue shades and MIS-2 with light yellow shades (bold line in C-H shows 3 point running averages). The 14C dates on the core are indicated by the red circles on the bottom axis.
- Figure: 3** Down core variations in (A) ratio of dissolution-susceptible species and dissolution-resistant species and (B) dissolution index from SSD-044/GC-01. The Last Glacial Maximum (LGM) is marked by dotted bars, and light yellow shades mark the Bølling Allerød (BA). The MIS-1 & MIS-3 marked by light green shade and MIS-2 with light pink shades (bold line in A and B show 3 point running averages).
- Figure: 4** Records of shell weights of (A) *G. ruber*, (B) *P. Obliquiloculata*, and (C) *N. dutertrei* from the core SSD-044/GC-01 during the last 43 ka. The MIS-1 & MIS-3 marked by light orange color shade and MIS-2 with light grey color (bold line in A-C show 3 point running averages).
- Figure: 5** Scanning electron micrograph (SEMs) of surface-dwelling planktic foraminifera *G. ruber* (size range 300-355) shells at a magnification of 700 × at (a) 8.31 kyr in the Holocene, (b) at 16.34 kyr in last deglacial and, (c) at ~21.76 ka in the LGM. The foraminifera shells display surface erosion, peeling, and dissolution of spines (marked by an ellipse) during LGM and Holocene, while well-preserved spines are seen in the deglacial sample.
- Table :1** The details of Accelerator Mass Spectrometer (AMS) 14C radiocarbon dates used to establish the chronology of the core SSD-044/GC-01.

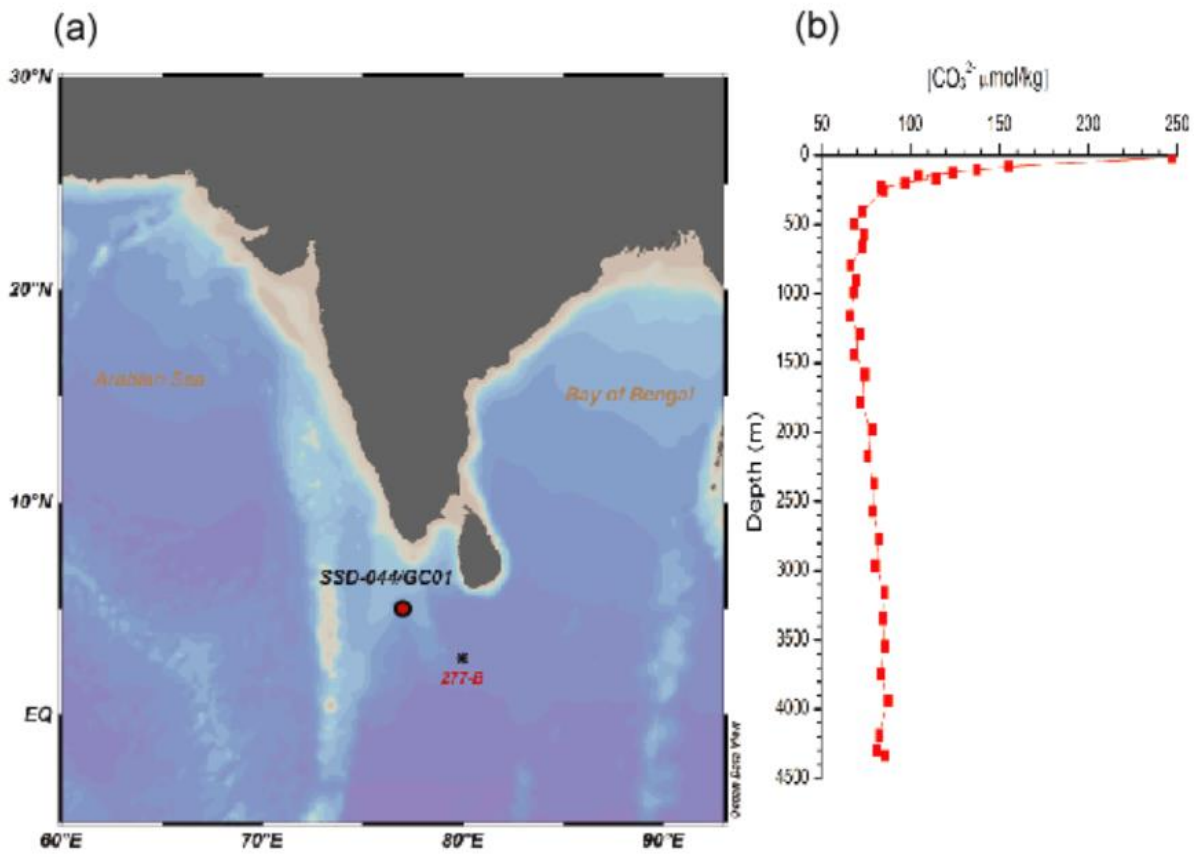


Figure 1

Figure 2

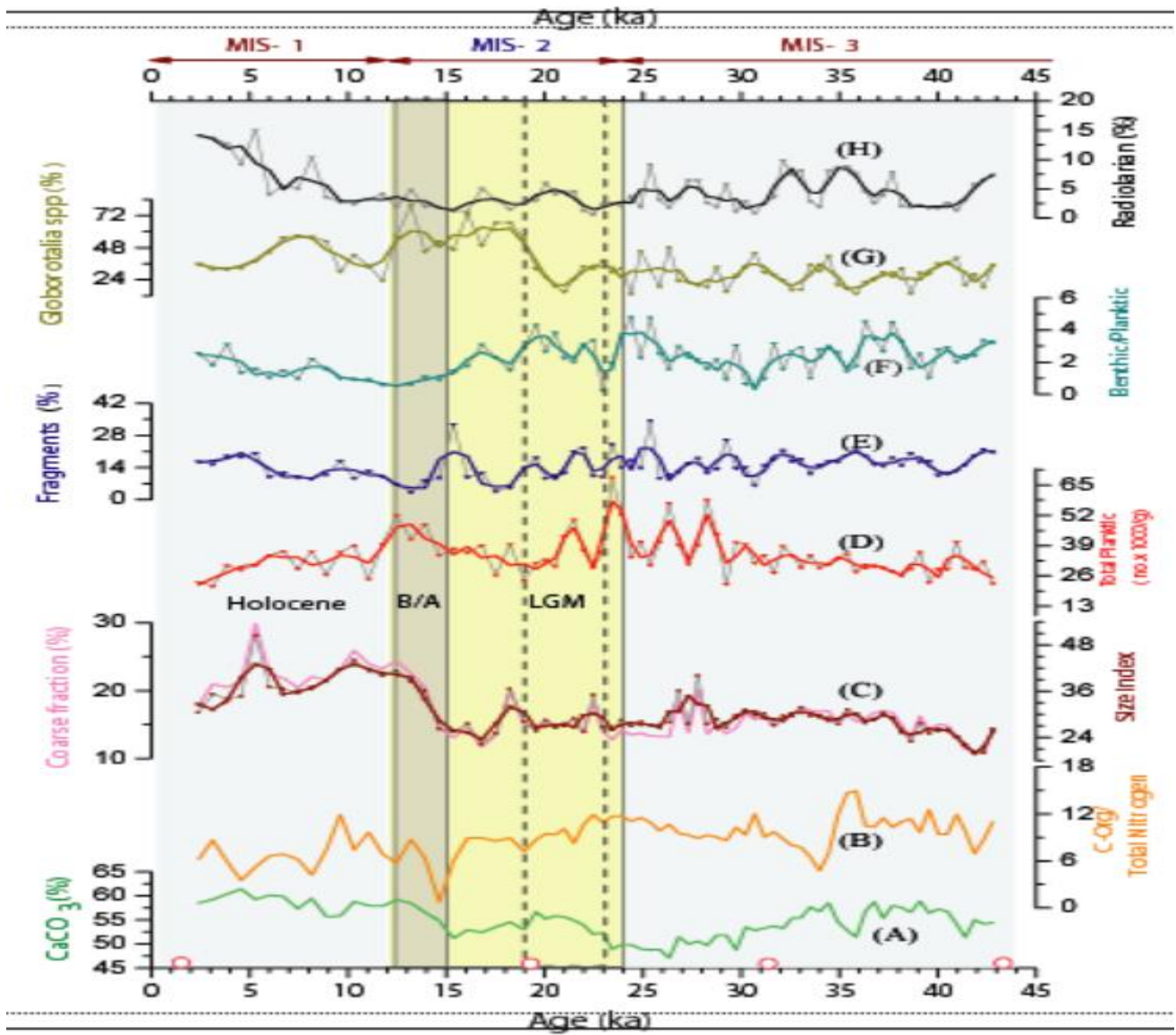


Figure 3

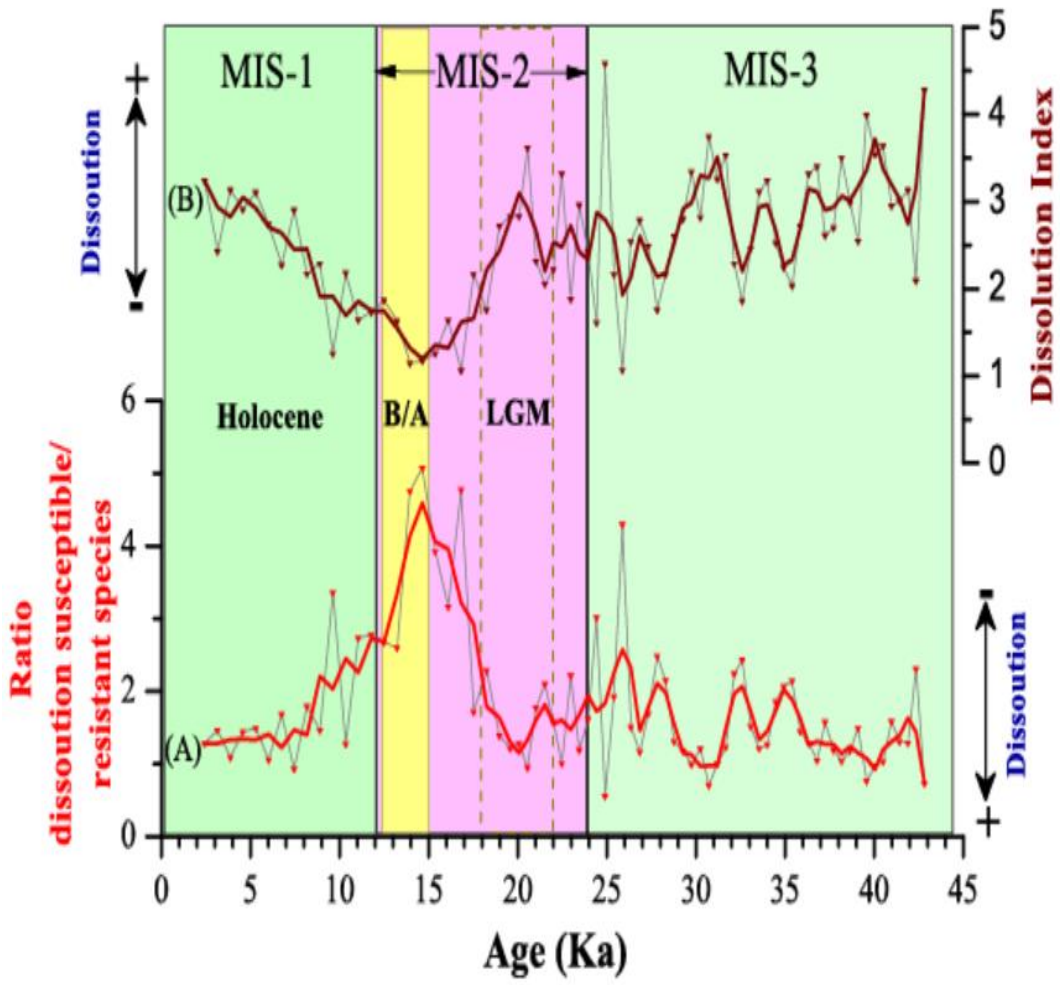


Figure 4

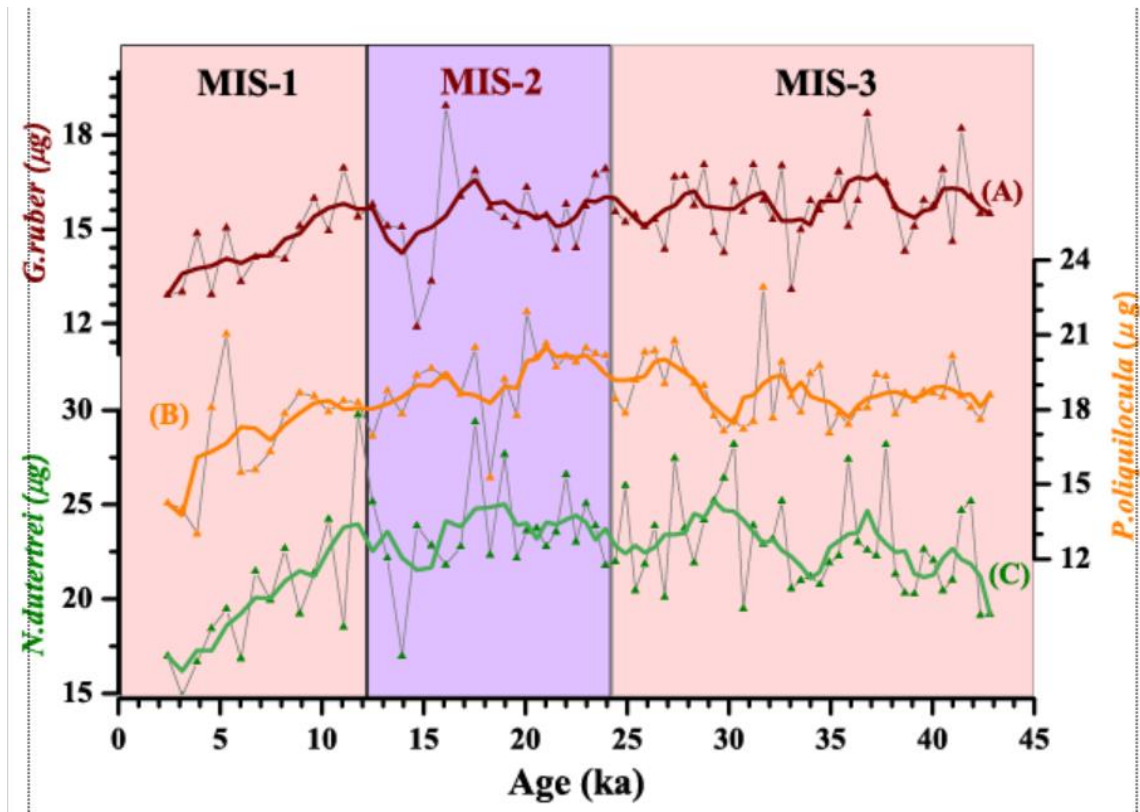
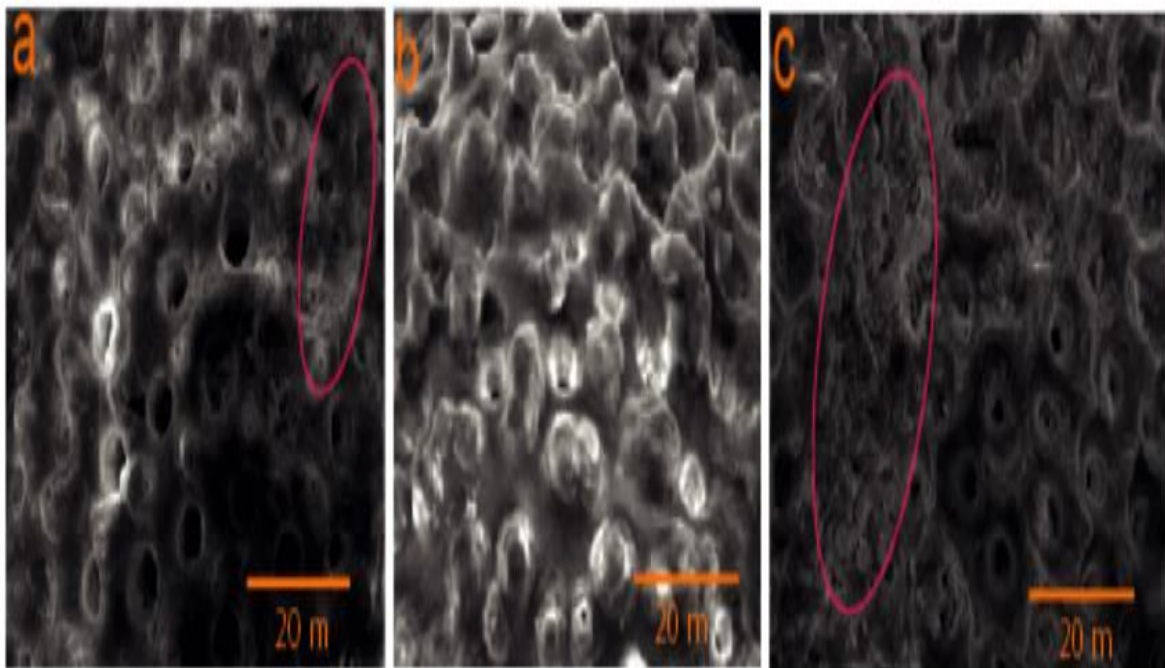


Figure 5





**Table 1**

S.No.	Depth (cm)	<sup>14</sup> C age	<sup>14</sup> C age error (±)	Calendar Years BP
1	1	2195	22	1704
2	50	16700	64	19336
3	100	28160	270	31449
4	150	40400	1200	43058

**Calib 8.2**

**Delta R = -77 (calculated using nearest 7 points)**

**Uncertainty = 58**